

THE PARAMETRIC DECAY INSTABILITY OF ALFVÉN WAVES IN TURBULENT PLASMAS AND THE APPLICATIONS IN THE SOLAR WIND

MIJIE SHI,^{1,2} HUI LI,² CHIJIE XIAO,¹ AND XIAOGANG WANG^{1,3}

¹*State Key Laboratory of Nuclear Physics and Technology, Fusion Simulation Center, School of Physics, Peking University, Beijing 100871, China*

²*Los Alamos National Laboratory, Los Alamos, New Mexico 87545, USA*

³*Department of Physics, Harbin Institute of Technology, Harbin 150001, China*

(Received ****; Revised ****; Accepted ****)

ABSTRACT

We perform three dimensional (3D) ideal magnetohydrodynamic (MHD) simulations to study the parametric decay instability of Alfvén waves in turbulent plasmas and explore its possible applications in the solar wind. We find that, over a broad range of parameters in background turbulence amplitudes, the parametric decay instability of an Alfvén wave with various amplitudes can still occur, though its growth rate in turbulent plasmas tends to be lower than both the theoretical linear theory prediction and that in the non-turbulent situations. Spatial - temporal FFT analyses of density fluctuations produced by the parametric decay instability match well with the dispersion relation of the slow MHD waves. This result may provide an explanation of the generation mechanism of slow waves in the solar wind observed at 1 AU. It further highlights the need to explore the effects of density variations in modifying the turbulence properties as well as in heating the solar wind plasmas.

Keywords: Alfvén waves — slow waves — parametric instability — solar wind

arXiv:1705.03829v1 [physics.space-ph] 10 May 2017

1. INTRODUCTION

The solar wind plasma is a natural laboratory to study processes relevant to space physics, plasma physics, as well as astrophysics (e.g., Tu & Marsch 1995; Bruno & Carbone 2013; Abbo et al. 2016). Spacecraft measurements show that the evolution of the solar wind is not adiabatically expanding, instead, additional heating effects are required during the expansion of the solar wind (e.g., Richardson et al. 1995; Richardson & Smith 2003). Numerous processes can heat the solar wind plasma, for example: dissipation of waves, stream interactions and shocks, pickup ions, etc. MHD waves, the low frequency (lower than ion cyclotron frequency Ω_{ci}) plasma waves, could play a significant role in heating both solar wind and solar corona (Chandran & Hollweg 2009; Ofman 2010; Cranmer & van Ballegoijen 2012). Among the three MHD waves, Alfvén waves have received the greatest attention because it is observed as the dominant component in the solar wind (Belcher & Davis 1971; Tu & Marsch 1995; Yan et al. 2016). There are some evidences that Alfvén waves also exist in the solar chromosphere and solar corona (De Pontieu et al. 2007; He et al. 2009; McIntosh et al. 2011). Alfvénic turbulence cascade has been well studied, where counter propagating Alfvén waves cascade and transfer energy from large scales to small scales and dissipate into heat (Tu et al. 1984; Goldreich & Sridhar 1995; Schekochihin et al. 2009).

The other two MHD waves, slow wave and fast wave, seem unlikely to exist in the solar wind plasma owing to the strong Landau damping (Barnes 1966; Barnes & Hung 1972; Barnes 1979). However, recent observations have shown the existence of slow waves. By analyzing the correlation between proton density and field aligned magnetic field, as well as the correlation's dependence on ion plasma β , Howes et al. (2012) showed the compressible components of solar wind turbulence are kinetic slow waves. Yao et al. (2013) found that some of the pressure balanced structures (Burlaga & Ogilvie 1970) in the solar wind are driven by oblique propagating slow waves, because oblique propagating slow waves suffer less from Landau damping (Barnes 1979) and may survive in the solar wind. Shi et al. (2015) identified some slow wave cases in the solar wind by dispersion relation comparison. He et al. (2015) observed the interaction between Alfvén waves and slow waves, and their effects on ion heating. Slow waves are also observed in the bursty flow of plasma sheet (Wang et al. 2016). Recently, Verscharen et al. (2017) found that the large scale compressible fluctuations in the solar wind are more like MHD slow modes than kinetic slow modes. As far as we know, the origin of slow waves in the solar wind is not clear. In this paper, we will propose a generation mechanism of slow waves in the solar wind turbulence.

In compressible plasmas, Alfvén waves will be subject to the parametric decay instability (PDI), during which forward propagating compressive fluctuations are produced and backward propagating Alfvén waves are also generated. Studies of PDI have a long history. For example, with a parallel propagating circularly polarized Alfvén wave in one-dimension, Derby (1978) and Goldstein (1978) derived a general dispersion relation for the growing compressive mode. Hollweg (1994) provided a derivation of different kinds of parametric instabilities. Dispersive effects were also introduced to study this process (Wong & Goldstein 1986). Many simulations for both monochromatic and non-monochromatic Alfvén waves with different polarizations have shown that the PDI of Alfvén waves is a robust process (e.g., Malara et al. 2000; Del Zanna et al. 2001; Del Zanna 2001; Matteini et al. 2010; Gao et al. 2013; Del Zanna et al. 2015). Furthermore, the PDI of Alfvén waves has been considered as an important mechanism to generate counter-propagating Alfvén waves, which are necessary for Alfvénic turbulence cascade, as well as to explain the decrease of cross helicity with the

increasing heliosphere distance (Roberts et al. 1987; Bavassano et al. 2000). Comparatively, however, the properties and consequences of the density fluctuations generated during the PDI of Alfvén wave are not studied in detail. It is possible that the density fluctuations may be partially responsible for producing the compressible slow modes in the solar wind.

In this work, we examine the applicability of the PDI of Alfvén waves in the solar wind by studying the propagation and dynamics of a single Alfvén wave in the turbulent background. By comparing the PDI of Alfvén waves in turbulent and non-turbulent situations, we find that the instability can still occur. In Section 2, we provide the simulation setup and results. In Section 3 we give the summary and discuss the possible applications.

2. SIMULATION RESULTS

2.1. Simulation Setup

Simulations are performed using the ideal MHD module of PLUTO code (Mignone et al. 2007). Two sets of simulations are performed which are categorized as turbulence simulations and non-turbulence simulations. The simulation domain is a 3D box elongated along the background magnetic field: $\mathbf{B}_0 = B_0 \hat{\mathbf{x}}$. Simulation domain is $[8\pi, 2\pi, 2\pi]$ and the grid size is $[1024, 256, 256]$ in x, y, z direction, respectively. Periodic boundary conditions are applied in all directions. In normalized units, $B_0 = 1, \rho_0 = 1$, Alfvén speed $v_A = 1$, sound speed $c_s = \sqrt{\gamma\beta/2}$, where β is the ratio between thermal pressure and magnetic pressure, and $\gamma = 5/3$ is the adiabatic index. Time is normalized by τ_A , where $\tau_A = 8\pi/v_A$ is Alfvén crossing time of the simulation domain along the $\hat{\mathbf{x}}$ direction.

For the turbulence simulations, we adopt a two-step process. First, we produce a turbulent background in the simulation domain following the procedure described in Makwana et al. (2015). Six linearly polarized Alfvén waves are injected into the domain, with their magnetic field and velocity perturbations in the following form,

$$\delta\mathbf{B}_{turb} = \sum_{j,k} \delta B_{turb} \cos(jk_x x + lk_z z + \phi_{j,l}) \hat{\mathbf{y}} + \sum_{m,n} \delta B_{turb} \cos(mk_x x + nk_y y + \phi_{m,n}) \hat{\mathbf{z}} \quad (1)$$

$$\delta\mathbf{v}_{turb} = - \sum_{j,k} \text{sgn}(j) \delta v_{turb} \cos(jk_x x + lk_z z + \phi_{j,l}) \hat{\mathbf{y}} - \sum_{m,n} \text{sgn}(m) \delta v_{turb} \cos(mk_x x + nk_y y + \phi_{m,n}) \hat{\mathbf{z}} \quad (2)$$

where $(j, l) = (1, 1), (1, 2), (-2, 3)$, $(m, n) = (-1, 1), (-1, -2), (2, -3)$, and $k_{x,y,z} = 2\pi/L_{x,y,z}$. Random phases are given by ϕ , and sgn is the sign function. There are three waves propagating obliquely in the positive $\hat{\mathbf{x}}$ and negative $\hat{\mathbf{x}}$ direction, respectively. The amplitudes δB_{turb} and δv_{turb} characterize the initial strength of the fluctuations and they also determine the magnitude of turbulence at later times when an Alfvén wave is injected. These counter-propagating Alfvén waves will cascade and form a decaying turbulent state. The turbulence is typically established after one Alfvén time (see Makwana et al. 2015, for details about the turbulence properties). Second, at $t = 1.2$, a circularly polarized Alfvén wave is injected into the domain with

$$\delta\mathbf{B}_{cir} = \delta B \cos(4x) \hat{\mathbf{y}} + \delta B \sin(4x) \hat{\mathbf{z}} \quad (3)$$

$$\delta\mathbf{v}_{cir} = -\delta\mathbf{B}_{cir} \quad (4)$$

where δB is the amplitude of the injected Alfvén wave and it has a wavenumber $k_{x0} = 4$. Simulations are typically extended to 4 Alfvén time to study the evolution of PDI. The power spectrum of B_z at

different times are shown in Figure 1. Before the Alfvén wave injection, the system has decayed to a turbulent state (blue line). After the injection of an Alfvén wave, a discrete mode at $k = 4$ with a relatively high power (corresponding to the injected Alfvén wave) is now visible in the spectrum (green line).

To our knowledge, all previous PDI studies were in the non-turbulence situation (e.g. Del Zanna et al. 2001). Typically, a circularly polarized Alfvén wave described by Equations 3 and 4 is injected into the simulation domain with a uniform background in density, pressure and magnetic field, plus a very small random density perturbations ($\delta\rho/\rho_0 \sim 10^{-2}$). This is what we used as well in non-turbulence simulations.

2.2. Parametric Decay Instability in Turbulence

The PDI of Alfvén waves is characterized by an exponential growth stage of the density fluctuations before saturation. In the one dimension (1D) limit, theoretical growth rates can be obtained from solving the dispersion relation derived by Derby (1978) and Goldstein (1978):

$$(\omega^2 - \beta k^2)(\omega + k + 2)(\omega + k - 2)(\omega - k) = \eta^2 k^2 (\omega^3 + k\omega^2 - 3\omega + k) \quad (5)$$

where ω and k are normalized by the frequency and wavenumber of the injected Alfvén wave and $\eta = \delta B/B_0$. Note that β in Equation 5 is defined as c_s^2/v_A^2 . Furthermore, for a given β and η , in multi-dimensional studies such as ours, we find that many oblique modes with different ω and \mathbf{k} are excited due to PDI.

Figure 2 (a) shows, in the non-turbulence simulations, the root mean square (RMS) density fluctuation evolution for different amplitudes δB of the injected Alfvén waves. The plasma $\beta = 0.5$ for all the simulations. An exponential growth stage is clearly seen for all simulations in Figure 2 (a), with the growth rate becoming larger when δB is larger. Note that even though the initial random density fluctuation amplitude is ~ 0.01 , it quickly drops below 10^{-3} , out of which PDI gradually grows. The growth of the RMS density is due to a single growing mode.

For the turbulence simulations with $\delta B_{turb} = \delta v_{turb} = 0.05$, the RMS density fluctuation evolution is shown in Figure 2 (b). The density fluctuation increases rapidly and remains nearly constant at ~ 0.01 during the cascade of Alfvén waves to develop turbulence. At $t = 1.2$, when a circularly polarized Alfvén wave is injected into the domain, the density fluctuation shows a sudden jump (most likely due to the ponderomotive effect of the injected wave), followed by an exponential growth stage. This is the signature that the injected Alfvén wave undergoes the parametric decay instability. The dependence of the PDI's growth rate on the amplitude of the injected waves can be seen from the slope changes during the exponential stage.

Figure 3 shows the evolution of density distribution in the $\{x, y\}$ plane ($z = \pi$) for a turbulence case with $\delta B = 0.2$ in Figure 2. After the injection of the circularly polarized Alfvén wave ((c) and (d) in Figure 3), the density mode shows a dominant mode with $k_x = 5$ and $k_y = k_z = 0$, which is exactly what the 1-D linear theory of PDI predicts with this parameter set. In addition, oblique slow modes with non-zero k_y and k_z are also developed, though with smaller growth rates. These results demonstrate that the PDI of a single Alfvén wave still occurs with the background turbulence, with both parallel and obliquely propagating slow modes (see below for detailed mode analysis).

To examine the mode growth in detail, we have carried out the FFT analysis of the density fluctuations and found that some modes exhibit exponential growth. Three of them ($\{k_x, k_y, k_z\} =$

$\{5, 0, 0\}, \{5, 0, 1\}, \{5, 1, 2\}$) are shown in Figure 4. We calculate the growth rates of the three modes in the time range between $t = 1.6$ and $t = 2.4$. The growth rates for the three modes are 0.024, 0.017, and 0.017, respectively, as shown in the legend of Figure 4. In particular, the mode $\{k_x, k_y, k_z\} = \{5, 0, 0\}$ (predicted by the linear theory) has the highest growth rate and is responsible for the most of the density RMS growth seen in Figure 2 (b). Figure 4 also shows two other modes ($\{k_x, k_y, k_z\} = \{4, 0, 0\}, \{6, 0, 0\}$), which have less energy than these PDI modes.

To quantitatively study the influence of turbulence on the growth rate of PDI, we have investigated two types of situations: one has the same background turbulence but different injected single Alfvén wave amplitudes and the other is the same injected Alfvén wave amplitudes but different background turbulence levels. We now discuss them in detail.

First, we present results from a suite of 3D simulations with the same turbulence background and the same single Alfvén wave injection time ($t = 1.2$) except that we vary the injected Alfvén wave amplitude, ranging from $\delta B/B = 0.1$ to 0.5. The plasma $\beta = 0.5$. The 1D linear theory predicts that the PDI mode with an integer wave-number should have $k_x = 5$ for all these parameters. From our non-linear 3D turbulence simulations, we confirm that indeed in all cases the maximum growth mode has $k_x = 5$. We then utilize the FFT analysis to select all the density modes with $k_x = 5$ and integrate over k_y and k_z . The growth rates are obtained during the exponential growth stage of their time histories.

Figure 5 shows the growth rate of PDI for different δB from three different situations: the 1-D linear theory, non-turbulence simulations and turbulence simulations with $\delta B_{turb} = 0.05$. The growth rates of non-turbulence simulations match the theoretical results with an error of less than 10%. The growth rates of turbulence simulations, however, are about half of the theoretical results. This suggests that the background turbulence has decreased the growth rate of PDI of Alfvén waves.

One interesting point worth noting is that, at $\delta B = 0.1$, the linear theory predicts there is no growth rate at the integer mode $k = 5$, though finite PDI growth is predicted for (non-integer) wavenumber very close to $k = 5$. Interestingly, both the turbulence and non-turbulence simulations show the growth of the $k_x = 5$ mode. We speculate that this is because the turbulence and/or the background fluctuations give rise to a “resonant broadening effect” (Dupree 1966) which produces a finite growth rate at $k_x = 5$.

Next, we show the evolution of PDI modes under different turbulence levels ($\delta B_{turb} = 0.05, 0.1, 0.15, 0.2$) and different amplitudes ($\delta B = 0.1$ to 0.5) of injected Alfvén waves in Figure 6. While the existence and the growth rate of PDI are relatively easy to quantify in many runs, it becomes difficult when the turbulence level is high and the PDI stage is relatively short. Figure 7 singles out the case with a fixed injected Alfvén wave amplitude ($\delta B = 0.4$) while varying the background turbulence level. This figure gives a clearer sense on the effects of the background turbulence. Overall, we find several trends: 1. The background turbulence levels do influence the growth rate of PDI. The growth rate decreases with increasing turbulence background. It is difficult to quantify the reduction for all cases due to the relatively short growth stage of PDI with high turbulence levels. 2. The background turbulence levels do influence the saturation level of PDI. Higher turbulence background gives lower saturation level of density variations from PDI. 3. Higher turbulence level also shortens the duration of the PDI stage. 4. In all the runs we have made so far, PDI nonetheless still gets excited. This demonstrates the robustness of this instability.

2.3. Generation of Slow Waves

Density fluctuations arise during the growth of PDI of Alfvén waves. To understand the nature of these fluctuations better, we employ the spatial-temporal FFT analysis to determine whether the density variations follow dispersion relations. For example, using the 3D simulation shown in Figure 2(b) with $\delta B = 0.2$, we put 50 time frames of 3D data together between $t = 2$ and 2.4 with a time resolution of $\delta t = 0.008$ to form a big 4D matrix. The FFT analysis of the matrix gives power P versus ω and k : $P(\omega, k_x, k_y, k_z)$. To get a clear view of the modes with the most power, we specify k_y, k_z and get a contour figure in the $\omega - k_x$ plane. These modes are then compared with the linearized ideal MHD modes for the same choices of k_y and k_z .

Figure 8 (a) shows the contour figure of FFT results of B_z in $\omega - k_x$ plane (with $k_y = 0, k_z = 0$), as well as the theoretical dispersion relation of three MHD waves. The Alfvén wave dispersion curve crosses the high power region exactly, indicating that this mode ($k_x = 4, k_y = k_z = 0$) is an Alfvén wave, which is actually the initial circularly polarized pump Alfvén wave. This result confirms that our method is reliable. To analyze the nature of the compressible modes, we perform the spatial-temporal FFT of density fluctuations $\delta\rho$ during the same time domain. Figure 8 (b) and (c) show the contours of two modes with high power, along with the theoretical dispersion relations of MHD waves. The mode in Figure 8 (b) propagates parallel to the background magnetic field and is either a slow wave or a sound wave (they are degenerate in this situation). Figure 8 (c) shows a mode with finite k_y and k_z , and it matches well with the dispersion relation of a slow wave. The growth rate of the slow modes in Figure 8 (b) and (c) is relatively large (see Figure 4). These results show that slow MHD waves are indeed generated via PDI.

3. SUMMARY AND CONCLUSION

We have performed 3D ideal MHD simulations to study the parametric decay instability of a circularly polarized Alfvén wave in both the turbulent and non-turbulent environments, and compare the growth rate of PDI in different situations. We find that in the turbulence circumstance, the PDI of Alfvén waves still occurs, though their growth rate is reduced to be about 50% of the growth rate predicted by the linear theory and confirmed by non-turbulence simulations. Because the growth time of the PDI modes typically last over $\sim 0.2 - 0.8 \tau_A$, the injected Alfvén wave could experience non-linear interactions with the background variations (such as Alfvén waves). The reduced growth rate of PDI in turbulent background may be related to these non-linear interactions, though further studies are needed to quantify this process. In addition, in certain cases, we find that the turbulence or background fluctuations can actually destabilize modes that are stable accordingly to the linear theory, an effect that seems to be similar to the resonance broadening process.

To study the nature of the compressible fluctuations generated during the PDI of Alfvén waves, we use the 4D spatial-temporal FFT method to analyze the density and magnetic field fluctuations, and compare the dispersion relations from simulations with those from theoretical MHD waves. Our results show that slow MHD waves are generated during the PDI. We propose that this mechanism can explain some of recent observations of slow waves in the solar wind (e.g., [Howes et al. 2012](#); [Yao et al. 2013](#); [He et al. 2015](#); [Shi et al. 2015](#)).

That slow waves can be produced by the PDI of Alfvén waves locally in the solar wind may have significant implications to understanding the solar wind heating. In addition to the often-considered scenario of Alfvénic cascade transferring energy to small scales where dissipation occurs, Alfvén waves at large scales may continuously transfer energy to compressible modes via PDI on relatively large scales, then the dissipation of these compressible modes via Landau damping can heat the solar wind

plasmas directly. Recently, [Schekochihin et al. \(2016\)](#) proposed an 'anti-phase-mixing' effect, which may suppress the damping and dissipation of compressible fluctuations in the turbulent background. It will be quite interesting to carry out further studies of these processes.

There are certain limitations of this work: We have used ideal MHD simulations that exclude Landau damping effect, which could affect the excitation of PDI in collisionless plasmas such as in the solar wind (e.g., [Araneda et al. 2008](#)). In addition, a continuously driven turbulence situation is more realistic for studying the evolution of PDI in relation to the solar wind. These effects are the subjects of future studies.

H. Li acknowledges useful discussions with B. Chandran. M. Shi thanks S. Li for his help in conducting MHD simulations. M. Shi and H. Li acknowledge the support by LANL/LDRD and DoE/OFES. Institutional computing resources were used for this study. This work is also supported by National Natural Science Foundation of China under 41274168, 40974104, 11375053 and ITER-CHINA program 2015GB120001, 2014GB107004. M. Shi is also supported by a scholarship from Graduate School of Peking University.

REFERENCES

- Abbo, L., Ofman, L., Antiochos, S. K., et al. 2016, *SSRv*, 201, 55
- Araneda, J. A., Marsch, E., & F.-Viñas, A. 2008, *Physical Review Letters*, 100, 125003
- Barnes, A. 1979, *J. Geophys. Res.*, 84, 4459
- Barnes, A. 1966, *Physics of Fluids*, 9, 1483
- Barnes, A., & Hollweg, J. V. 1974, *J. Geophys. Res.*, 79, 2302
- Barnes, A., & Hung, R. J. 1972, *Journal of Plasma Physics*, 8, 197
- Bavassano, B., Pietropaolo, E., & Bruno, R. 2000, *J. Geophys. Res.*, 105, 12697
- Belcher, J. W., & Davis, L., Jr. 1971, *J. Geophys. Res.*, 76, 3534
- Bruno, R., & Carbone, V. 2013, *Living Reviews in Solar Physics*, 10, 7
- Burlaga, L. F., & Ogilvie, K. W. 1970, *SoPh*, 15, 61
- Chandran, B. D. G., & Hollweg, J. V. 2009, *ApJ*, 707, 1659
- Cranmer, S. R., & van Ballegooijen, A. A. 2012, *ApJ*, 754, 92
- De Pontieu, B., McIntosh, S. W., Carlsson, M., et al. 2007, *Science*, 318, 1574
- Del Zanna, L., Matteini, L., Landi, S., Verdini, A., & Velli, M. 2015, *Journal of Plasma Physics*, 81, 325810102
- Del Zanna, L., Velli, M., & Londrillo, P. 2001, *A&A*, 367, 705
- Del Zanna, L. 2001, *Geophys. Res. Lett.*, 28, 2585
- Derby, N. F., Jr. 1978, *ApJ*, 224, 1013
- Dupree, T. H. 1966, *Physics of Fluids*, 9, 1773
- Gao, X., Lu, Q., Li, X., Shan, L., & Wang, S. 2013, *Physics of Plasmas*, 20, 072902
- Goldreich, P., & Sridhar, S. 1995, *ApJ*, 438, 763
- Goldstein, M. L. 1978, *ApJ*, 219, 700
- He, J.-S., Tu, C.-Y., Marsch, E., et al. 2009, *A&A*, 497, 525
- He, J., Tu, C., Marsch, E., et al. 2015, *ApJL*, 813, L30
- Hollweg, J. V. 1994, *J. Geophys. Res.*, 99, 23
- Howes, G. G., Bale, S. D., Klein, K. G., et al. 2012, *ApJL*, 753, L19
- Makwana, K. D., Zhdankin, V., Li, H., Daughton, W., & Cattaneo, F. 2015, *Physics of Plasmas*, 22, 042902
- Malara, F., Primavera, L., & Veltri, P. 2000, *Physics of Plasmas*, 7, 2866
- Matteini, L., Landi, S., Del Zanna, L., Velli, M., & Hellinger, P. 2010, *Geophys. Res. Lett.*, 37, L20101
- McIntosh, S. W., de Pontieu, B., Carlsson, M., et al. 2011, *Nature*, 475, 477
- Mignone, A., Bodo, G., Massaglia, S., et al. 2007, *ApJS*, 170, 228
- Ofman, L. 2010, *Living Reviews in Solar Physics*, 7

- Richardson, J. D., Paularena, K. I., Lazarus, A. J., & Belcher, J. W. 1995, *Geophys. Res. Lett.*, 22, 325
- Richardson, J. D., & Smith, C. W. 2003, *Geophys. Res. Lett.*, 30, 1206
- Roberts, D. A., Goldstein, M. L., Klein, L. W., & Matthaeus, W. H. 1987, *J. Geophys. Res.*, 92, 12023
- Schekochihin, A. A., Cowley, S. C., Dorland, W., et al. 2009, *ApJS*, 182, 310
- Schekochihin, A. A., Parker, J. T., Highcock, E. G., et al. 2016, *Journal of Plasma Physics*, 82, 905820212
- Shi, M. J., Xiao, C. J., Li, Q. S., et al. 2015, *ApJ*, 815, 122
- Tu, C.-Y., & Marsch, E. 1995, *SSRv*, 73, 1
- Tu, C.-Y., Pu, Z.-Y., & Wei, F.-S. 1984, *J. Geophys. Res.*, 89, 9695
- Verscharen, D., Chen, C. H. K., & Wicks, R. T. 2017, [arXiv:1703.03040](https://arxiv.org/abs/1703.03040)
- Wang, T., Cao, J., Fu, H., Meng, X., & Dunlop, M. 2016, *Geophys. Res. Lett.*, 43, 1854
- Wong, H. K., & Goldstein, M. L. 1986, *J. Geophys. Res.*, 91, 5617
- Yan, L., He, J., Zhang, L., et al. 2016, *ApJL*, 816, L24
- Yao, S., He, J.-S., Tu, C.-Y., Wang, L.-H., & Marsch, E. 2013, *ApJ*, 774, 59

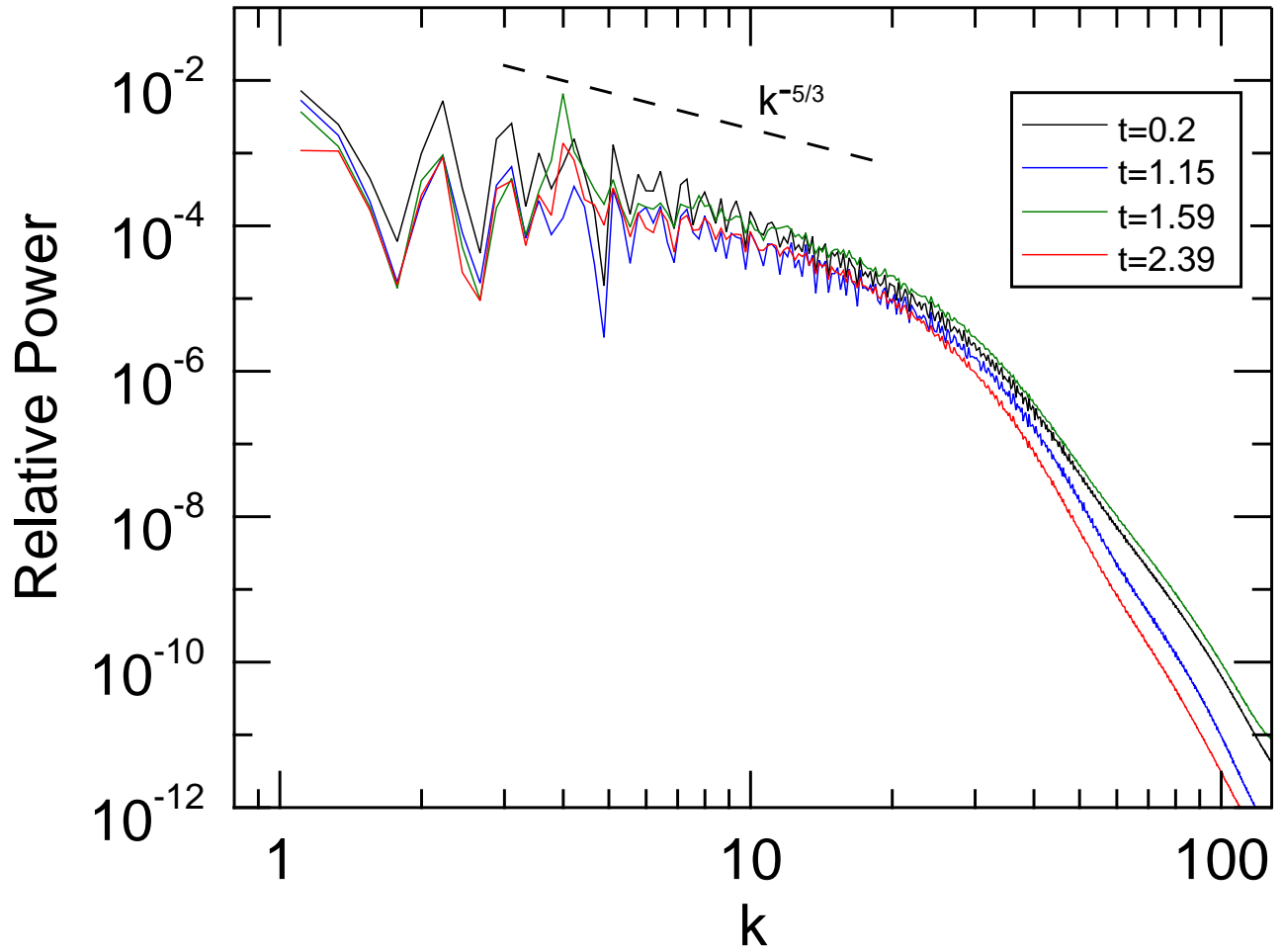


Figure 1. Power spectrum of B_z component at different times of one turbulence simulation ($\delta B_{turb} = \delta v_{turb} = 0.15$). The spectrum is normalized by the grids size. At $t = 1.2$, an Alfvén wave with $\delta B = 0.2$ is injected into the simulation domain.

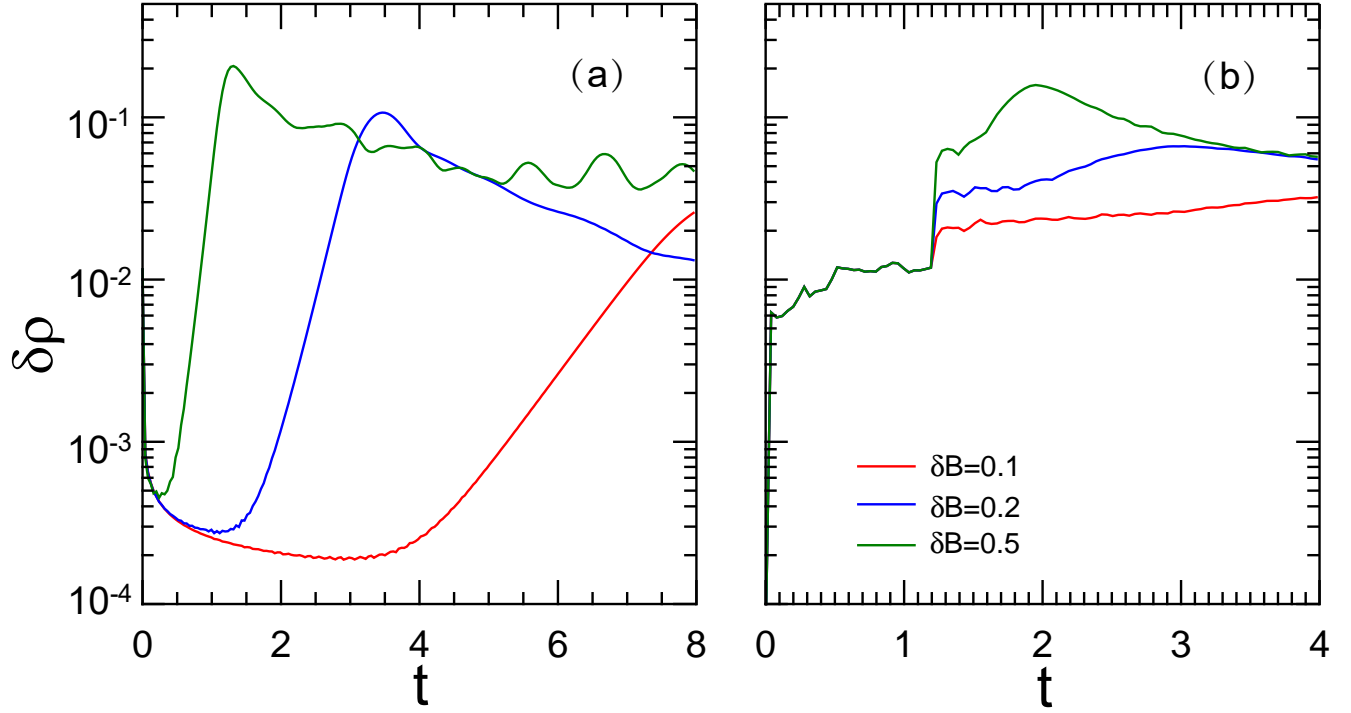


Figure 2. Evolution of root mean square (RMS) density fluctuation for (a) non-turbulence simulations and (b) turbulence simulations ($\delta B_{turb} = \delta v_{turb} = 0.05$). Red, blue, and green lines are for $\delta B = 0.1, 0.2$, and 0.5 , respectively. Plasma $\beta = 0.5$ for all simulations. At $t = 1.2\tau_A$, an Alfvén wave is injected into the domain in turbulence simulations.

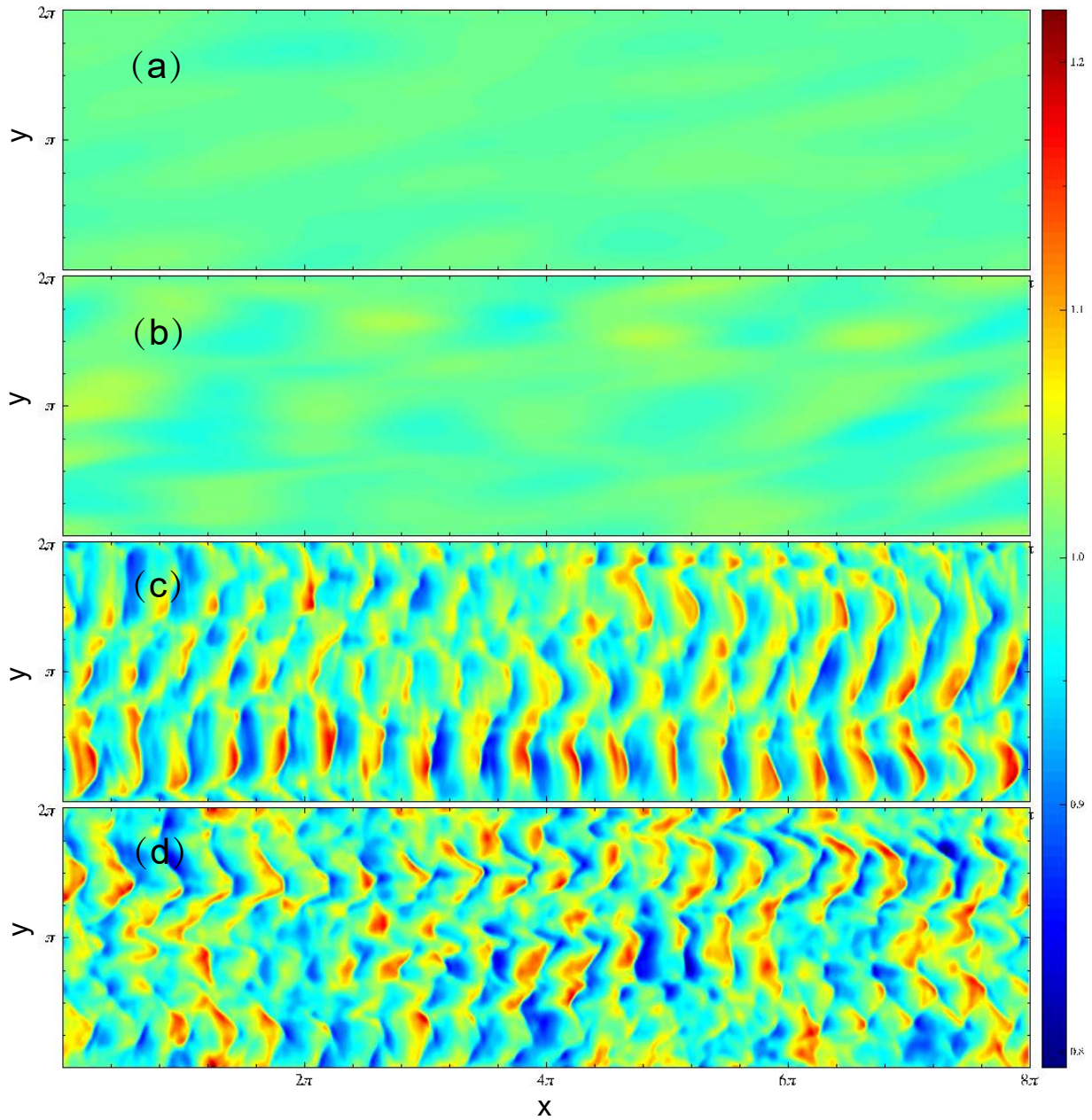


Figure 3. Evolution of density distribution in the $\{x, y\}$ plane ($z = \pi$) for a turbulence case with $\delta B = 0.2$ at (a) $t = 0.08$, (b) $t = 1.15$, (c) $t = 2.39$, and (d) $t = 3.98$. An Alfvén wave is injected at $t = 1.2$.

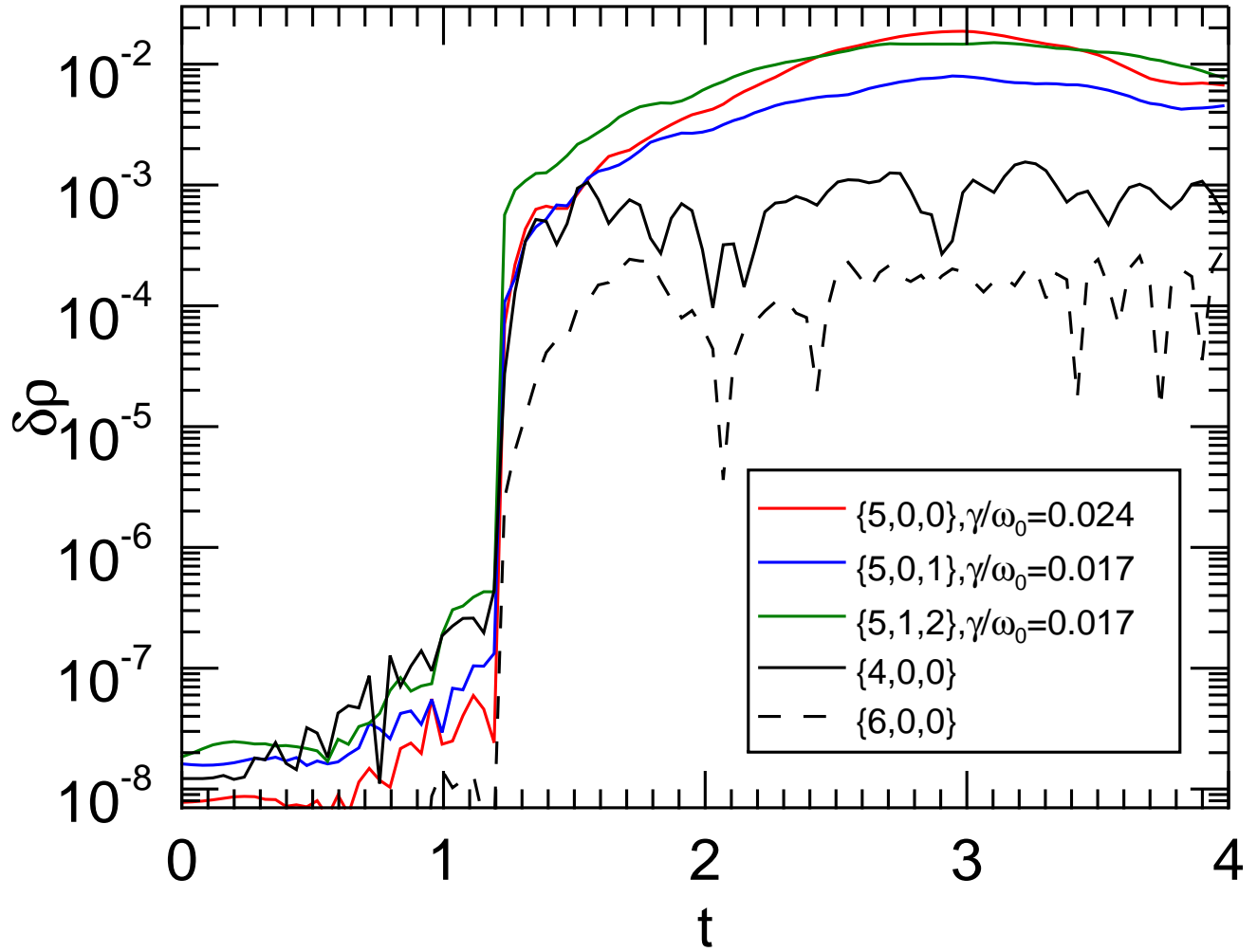


Figure 4. Evolution of RMS density fluctuation of three PDI modes $\{k_x, k_y, k_z\} = \{5, 0, 0\}$, $\{5, 0, 1\}$, and $\{5, 1, 2\}$ as well as two other modes $\{k_x, k_y, k_z\} = \{4, 0, 0\}$, $\{6, 0, 0\}$. The growth rates of PDI modes are labeled in the legends. A circularly polarized Alfvén wave with $\delta B = 0.2$ is injected at $t = 1.2$.

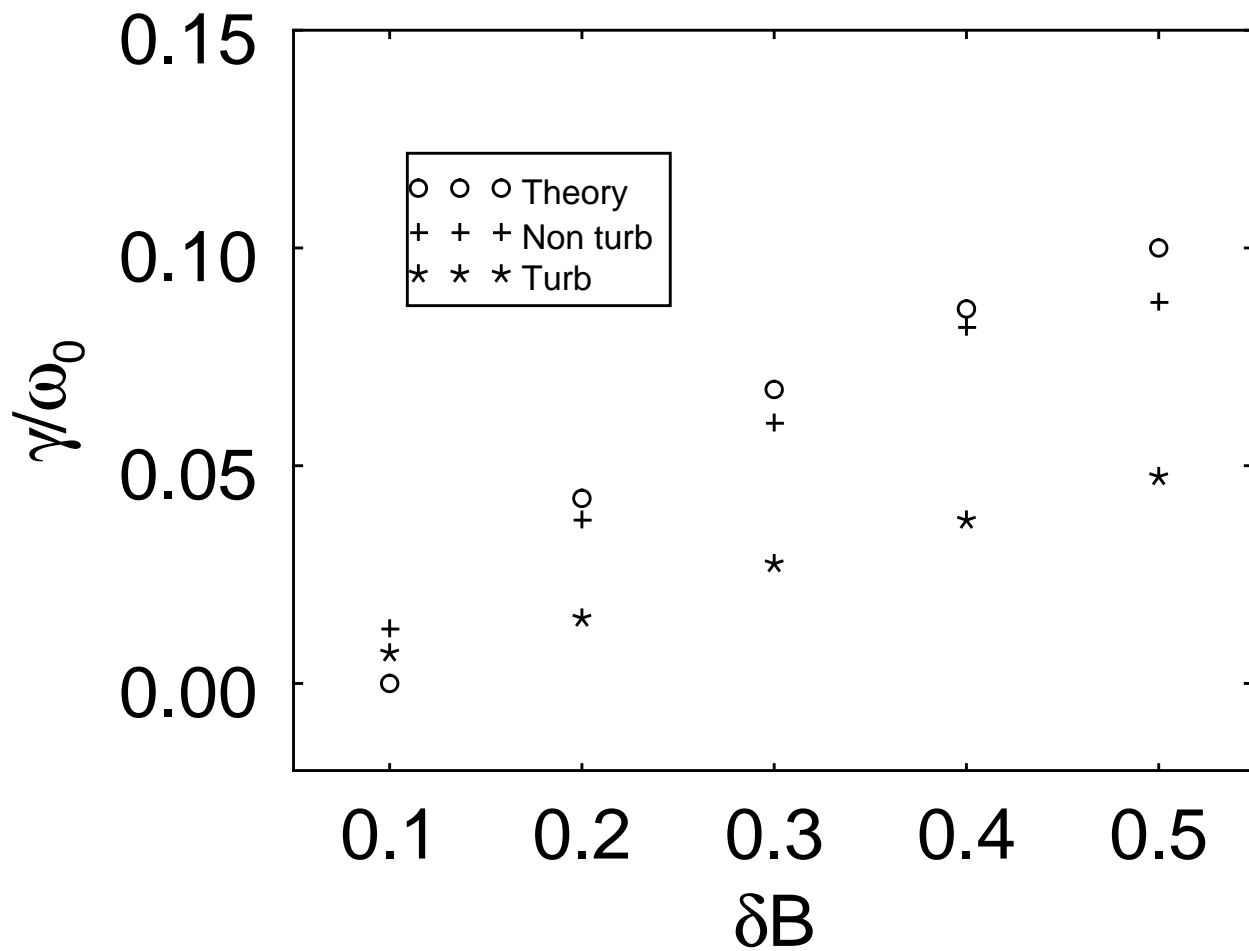


Figure 5. Growth rate comparison of PDI modes for turbulence simulations (\star) ($\delta B_{turb} = \delta v_{turb} = 0.05$), non-turbulence simulations (+), and theoretical predictions (\circ) from Equation 5, with different amplitudes of circularly polarized Alfvén waves. The plasma $\beta = 0.5$.

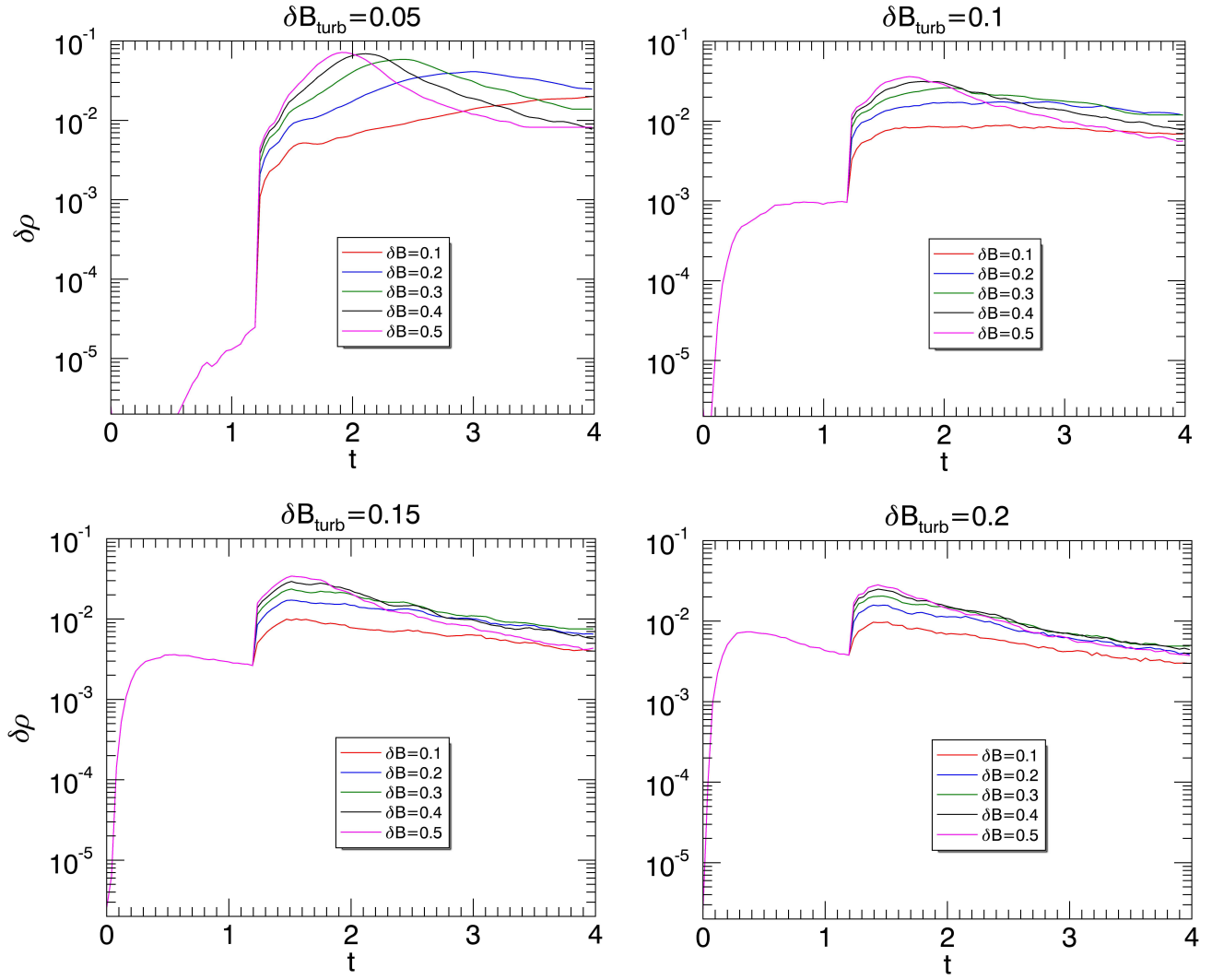


Figure 6. Evolution of PDI modes under different background turbulence levels (δB_{turb}) and different amplitudes of injected Alfvén waves (δB). A circularly polarized Alfvén wave is injected at $t = 1.2$.

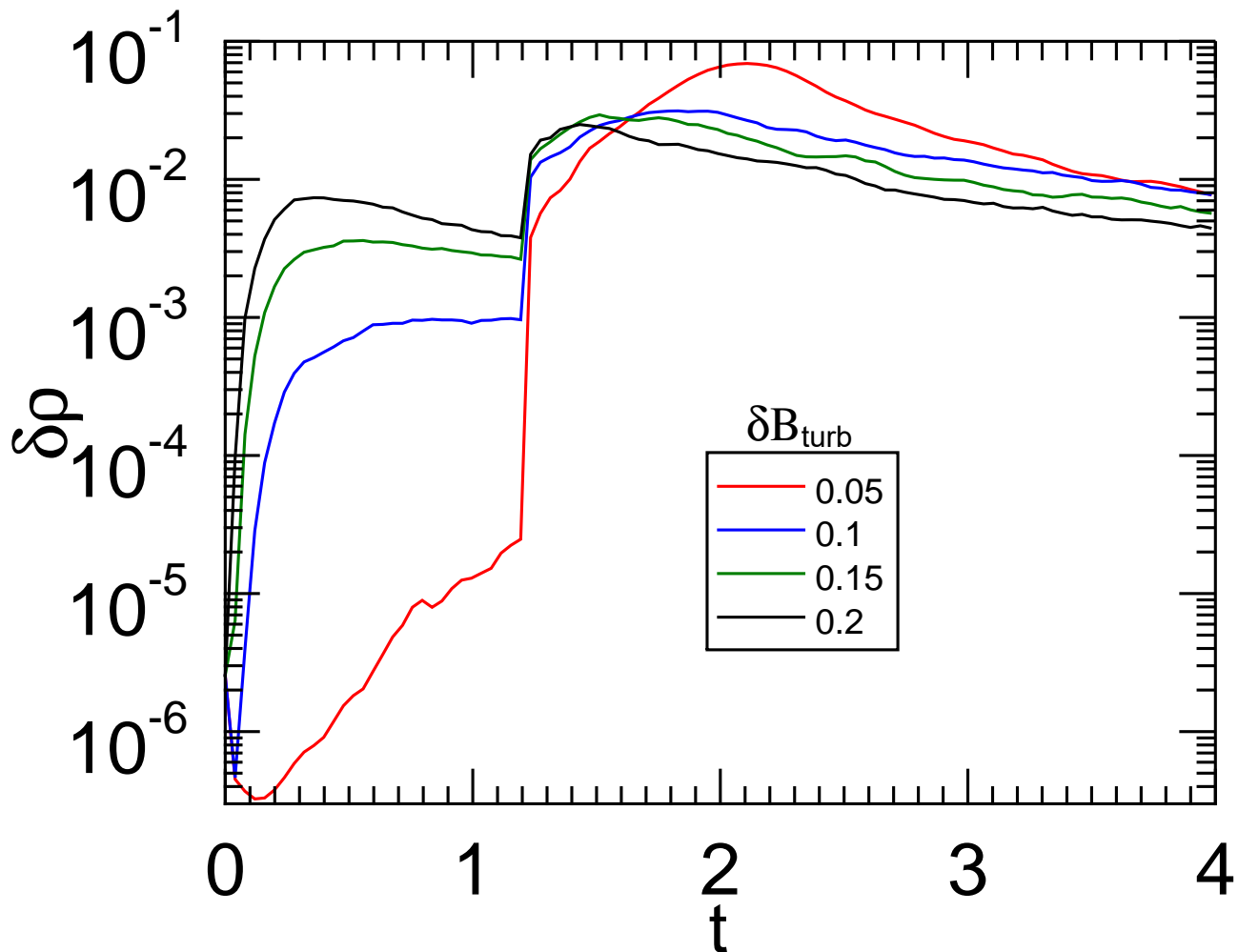


Figure 7. Evolution of PDI modes in different background turbulence levels (δB_{turb}). A circularly polarized Alfvén wave with $\delta B = 0.4$ is injected at $t = 1.2$.

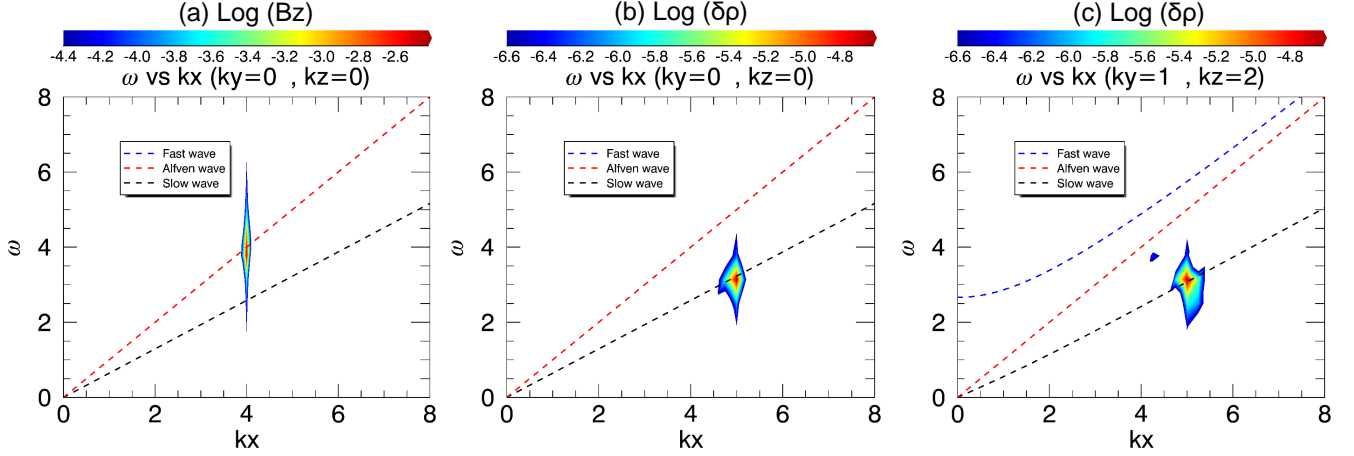


Figure 8. (a) Contour of mode $(k_x, k_y, k_z = 4, 0, 0)$ from spatial-temporal FFT results of B_z (the injected Alfvén wave), as well as the theoretical dispersion relations of fast (blue), Alfvén (red), and slow (black) waves. Note that fast wave and Alfvén wave are degenerate in this situation. (b) Contour of mode $(k_x, k_y, k_z = 5, 0, 0)$ from spatial-temporal FFT results of $\delta\rho$, as well as the theoretical dispersion relations of fast (blue), Alfvén (red), and slow (black) waves. (c) Contour of mode $(k_x, k_y, k_z = 5, 1, 2)$ from spatial-temporal FFT results of $\delta\rho$, as well as the theoretical dispersion relations of fast (blue), Alfvén (red), and slow (black) waves. Analyses uses the simulation data from $t = 2$ and 2.4 , $\beta = 0.5$, and $\delta B = 0.2$.